Key Engineering Materials
ISSN: 1662-9795, Vol. 926, pp 1108-1121
doi:10.4028/p-0873q9
© 2022 The Author(s). Published by Trans Tech Publications Ltd, Switzerland.
Submitted: 2021-12-08
Revised: 2022-01-17
Accepted: 2022-02-04
Online: 2022-07-22

On the Effect of the Tension-Compression Ratio on Forming of Isotropic Materials

Marta C. Oliveira[1,a*], Ivan Prcela[2,b], Vedrana Cvitanić[2,c], Diogo M. Neto[1,d], José L. Alves[3,e] and Luís F. Menezes[1,f]

[1]CEMMPRE, Department of Mechanical Engineering, University of Coimbra, Pinhal de Marrocos, 3030-788 Coimbra, Portugal

[2]Department of Mechanical Engineering and Naval Architecture, University of Split, Rudjera Boskovica 32, 21 000 Split, Croatia

[3]Microelectromechanical Systems Research Unit, University of Minho, Campus de Azurém, Guimarães, 4800-058, Portugal

[a]marta.oliveira@dem.uc.pt, [b]Ivan.Prcela.00@fesb.hr, [c]vcvit@fesb.hr, [d]diogo.neto@dem.uc.pt, [e]jlalves@dem.uminho.pt, [f]luis.menezes@dem.uc.pt,

Keywords: Finite element method, Isotropic yield function, Tension-compression asymmetry.

Abstract. It is generally believed that the choice of the yield criterion used to describe the plastic behaviour of isotropic metallic materials does not affect much the accuracy of the predictions of forming operations. For this reason, the von Mises yield criterion is widely used for modelling their plastic behaviour. However, according to the von Mises yield criterion, the ratio between the yield stresses in tension and compression is always 1.0. Nevertheless, materials can present same asymmetry, i.e. a strength differential (SD) effect. In this work, the yield criterion proposed by Cazacu et al. [1], is adopted to describe the mechanical behaviour of isotropic materials, with different levels of tension-compression asymmetry. Numerical simulations of the deep drawing of a cylindrical cup were performed considering these different virtual isotropic materials, in order to evaluate its impact on the thickness distribution and cup height. The analysis of the stress and strain paths, for material points initially located in the flange is performed, enabling the correlation between the thickness distributions predicted and the plastic strain ratios obtained analytically, using the yield function and the normality rule. The results show that even small changes in the tension-compression stress ratio can influence the strains distribution, in isotropic materials.

Introduction

The analysis of the mechanical behaviour of isotropic metallic materials is commonly performed with the von Mises yield criterion. This yield criterion is widely adopted because it renders a quadratic yield surface, which enables an easier implementation in finite element codes than, for instance the Tresca yield criterion. An associated flow rule is commonly adopted, meaning that the yield surface also defines the direction of the plastic strain rate. When comparing the yield surfaces defined by von Mises and Tresca yield criteria, although the yield stress for tension, compression and equibiaxial stress states are equal, the yield stress in shear and plane strain are different. Moreover, the direction of the plastic strain rate is equal for all these stress states, but evolves differently between them. Therefore, their application to the numerical simulation of a cylindrical cup results in different cup heights, which is connected with different thickness distributions along the cup wall. This confirms the influence of the yield surface shape on the strain distribution when adopting an associated flow rule. Moreover, some materials also present tension-compression asymmetry, i.e. the yield stress in tension is lower/higher than the yield stress in compression. Some yield criteria have been proposed in order to describe this behaviour, also called strength differential (SD) effect. An example is the one proposed by Cazacu, Plunkett and Barlat (2006) [1], which is used in this work and labelled in the following as CPB06. For a material showing no SD effect, the CPB06 yield criterion reduces to the von Mises one. This allows the qualitative and quantitative analysis of the impact of the level of tension-compression asymmetry on the numerical results in the forming of a cylindrical cup. This

This article is an open access article under the terms and conditions of the Creative Commons Attribution (CC BY) license
(https://creativecommons.org/licenses/by/4.0)

example is selected in this study because the sheet is submitted to different stress states, meaning that the numerical results are sensitive to small changes in the yield surface shape [2], enabling an improved understanding of the influence of the SD effect. Furthermore, most metallic sheets exhibit orthotropic plastic behaviour, but since the influence of SD effect is analysed, in the performed numerical simulations virtual isotropic materials are utilized.

In the following section, the CPB06 yield criterion is briefly described. The yield surfaces describing the mechanical behaviour of virtual isotropic materials, with different levels of tension-compression asymmetry, are analysed as well as the impact of the SD effect on the direction of the plastic strain rate.

Cazacu, Plunkett and Barlat (2006) Isotropic Yield Criterion

Cazacu, Plunkett and Barlat (2006) proposed an isotropic yield criterion of the form:

$$G\left(s_1,s_2,s_3,k,a\right)=\left(\left|s_1\right|-ks_1\right)^a+\left(\left|s_2\right|-ks_2\right)^a+\left(\left|s_3\right|-ks_3\right)^a=\bar{\sigma}^a\,, \tag{1}$$

to account for yielding asymmetry, between tension and compression, associated either with deformation twinning or with non-Schmidt effects at single crystal level. In the above equation, s_i, with $i=1,2,3$, are the principal values of the stress deviatoric component of the Cauchy stress tensor. a and k are material parameters and $\bar{\sigma}$ is the equivalent stress. It was shown that for a fixed value of the exponent a, the parameter k is expressible solely in terms of the ratio $\sigma^{\mathrm{T}}/\sigma^{\mathrm{C}}$, where σ^{T} and σ^{C} are the uniaxial yield stress in tension and in compression, respectively. The expression that relates k with this ratio is as follows

$$k=\frac{1-h\left(\sigma^{\mathrm{T}}/\sigma^{\mathrm{C}}\right)}{1+h\left(\sigma^{\mathrm{T}}/\sigma^{\mathrm{C}}\right)}\ \text{with}\ h\left(\frac{\sigma^{\mathrm{T}}}{\sigma^{\mathrm{C}}}\right)=\left(\frac{2^a-2\left(\sigma^{\mathrm{T}}/\sigma^{\mathrm{C}}\right)^a}{\left(2\sigma^{\mathrm{T}}/\sigma^{\mathrm{C}}\right)^a-2}\right)^{1/a}. \tag{2}$$

Irrespective of the value of a, if the yield stresses in tension and compression are equal ($\sigma^{\mathrm{T}}=\sigma^{\mathrm{C}}$), meaning that the parameter k is equal to zero. In particular, for $k=0$ and $a=2$, the yield criterion defined by Eq. (1) reduces to the von Mises yield criterion. The convexity of the yield surface is guaranteed for any integer $a\geq 2$ and $k\in\left[-1;1\right]$ [1]. In this work, a constant B is adopted, such that the yield stress reduces to the tensile stress. Thus, the loading condition imposes that the equivalent stress is equal to the yield stress Y, written as:

$$Y=B\left[\left(\left|s_1\right|-ks_1\right)^a+\left(\left|s_2\right|-ks_2\right)^a+\left(\left|s_3\right|-ks_3\right)\right]^{1/a}, \tag{3}$$

where

$$B=\left(\frac{1}{\left(\left(2/3\right)\left(1-k\right)\right)^a+2\left(\left(1/3\right)\left(1+k\right)\right)^a}\right)^{1/a}. \tag{4}$$

The physical significance of the material parameter k may be revealed from uniaxial tests. Indeed, according to Eq. (3), the ratio of tensile to compressive uniaxial yield stress is given by [1]

$$\frac{\sigma^{\mathrm{T}}}{\sigma^{\mathrm{C}}}=\left[\frac{\left(\left(2/3\right)\left(1+k\right)\right)^a+2\left(\left(1/3\right)\left(1-k\right)\right)^a}{\left(\left(2/3\right)\left(1-k\right)\right)^a+2\left(\left(1/3\right)\left(1+k\right)\right)^a}\right]^{1/a}. \tag{5}$$

It can be shown that this ratio is equal to the one obtained between the yield stress in uniaxial tension and equibiaxial tension, σ_b^T. It follows that according to this criterion, the yield stress in uniaxial compression and equibiaxial tension are equal $\sigma_b^T = \sigma^C$. On the other hand, the yield stress in biaxial compression, σ_b^C, is always equal to the yield stress in uniaxial tension, i.e. $\sigma_b^C = \sigma^T$. Finally, the ratio between the yield stress in uniaxial tension and in shear, τ, is given as follows [1]:

$$\frac{\sigma^T}{\tau} = \left[\frac{(1+k)^a + (1-k)^a}{\left((2/3)(1-k)\right)^a + 2\left((1/3)(1+k)\right)^a} \right]^{1/a} . \tag{6}$$

The variation of σ^T/σ^C with k is illustrated in Fig. 1 a) for different values of the exponent a. Note that according with Eq. (5):

- For $k=-1$, $\sigma^T/\sigma^C = 2^{(1-a)/a}$.
  Thus, when $a=2$, $\sigma^T/\sigma^C = 1/\sqrt{2}$ and when $a \to \infty$, $\sigma^T/\sigma^C = 1/2$.
- For $k=1$, $\sigma^T/\sigma^C = 2^{(a-1)/a}$.
  Thus, when $a=2$, $\sigma^T/\sigma^C = \sqrt{2}$ and when $a \to \infty$, $\sigma^T/\sigma^C = 2$.

The variation of σ^T/τ with k is illustrated in Fig. 1 b) for different values of the exponent a. Note that according with Eq. (6):

- For $k=0$ and $a=2$, $\sigma^T/\tau = \sqrt{3}$ (von Mises).
- For $k=-1$, $\sigma^T/\tau = 3/2$.
  Thus, the ratio is independent of the exponent a.
- For $k=1$, $\sigma^T/\tau = \left(3^a/2\right)^{1/a}$.
  Thus, when $a=2$, $\sigma^T/\tau = \sqrt{9/2}$ and when $a \to \infty$, $\sigma^T/\tau = 3$.

From Figs. 1 a) and b) it can be observed that for k values obeying the convexity condition, a wider stress ratio range is covered for greater values of exponent a.

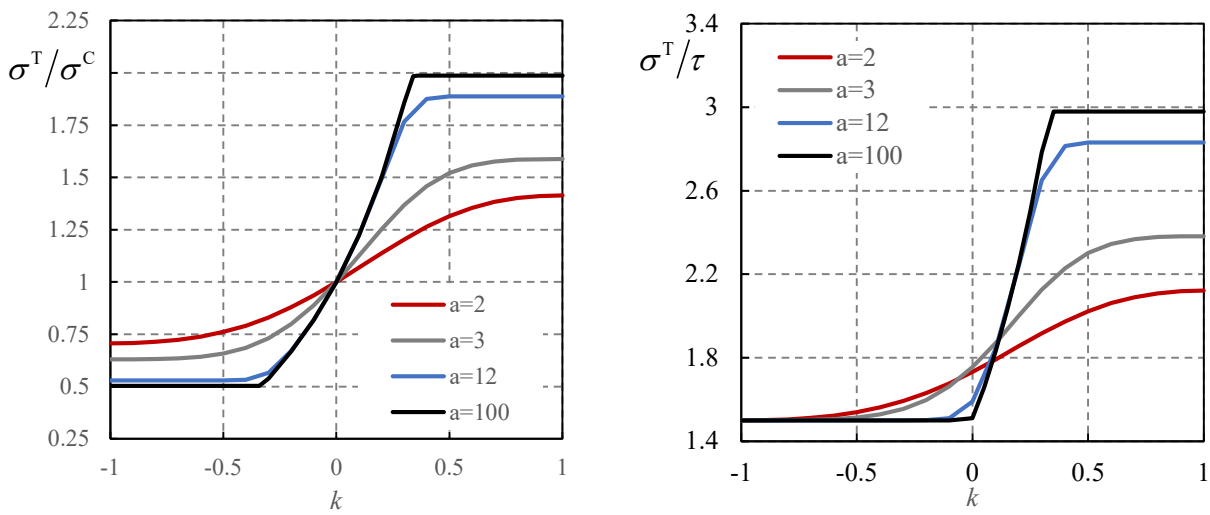

a) b)

Fig. 1 – The influence of the value of the parameter k on the ratio: a) σ^T/σ^C and b) σ^T/τ, for various values of the exponent a.

Fig. 2 a) shows the projection of the yield surface, given by Eq. (3), in the biaxial plane (i.e. a plane corresponding to one of the eigenvalues of the Cauchy stress tensor being equal to zero), for several values of yield stress ratios σ^T/σ^C and $a=2$. The corresponding k values are presented in Table 1. In this figure, the non-null principal stresses are denoted as σ_1 and σ_2. This is done in order to facilitate the discussion and analysis of the forming results presented in the simulation chapter.

The centre surface (black line) corresponds to $\sigma^T/\sigma^C =$ 1, i.e. von Mises. The other surfaces are something between ellipsoidal (closer to von Mises) and triangle-like. In fact, the surface is isosceles triangle-like with rounded edges, with the "tip" of the triangle in the biaxial tension stress state for

stress ratios $\sigma^{T}/\sigma^{C} < 1$ and in the opposite direction for stress ratios $\sigma^{T}/\sigma^{C} > 1$. This is related with the fact that the yield stress in biaxial tension is always equal to the yield stress in compression and the yield stress in biaxial compression is always equal to the yield stress in tension. With the introduction of the normalization parameter B (see Eq. (3)), all yield surfaces share the same yield stress in uniaxial tension (in both principal directions, because the material is isotropic). The change of the σ^{T}/σ^{C} ratio, leads to lower yield stress in tension than in compression for $k < 0$, while the opposite happens for $k > 0$. Thus, for $k < 0$ $\left(\sigma^{T}/\sigma^{C} < 1\right)$ the yield surface is exterior to the von Mises one, while the opposite happens for $k > 0$ $\left(\sigma^{T}/\sigma^{C} > 1\right)$. This will have impact in the energy required to deform the material, as discussed in the analysis of the results. Fig. 2 b) shows the projection of the yield surface, given by Eq. (3), in the biaxial plane, for several values of yield stress ratios σ^{T}/σ^{C} and $a = 12$. Note that the yield stress ratios selected are identical to the ones used for $a = 2$, although the possible range is wider (see Fig. 1 a)). The corresponding k values are presented in Table 1. It can be seen that for $a = 12$ all yield surfaces have a triangle-like shape. The figure highlights that the differences in the yield surface shape for $a = 2$ and $a = 12$ are marginal for the extreme stress ratio values. In fact, the differences are more pronounced for the medium values (stress ratio around 1). Anyway, the surfaces with $a = 2$ are always interior to the ones with $a = 12$ and the same σ^{T}/σ^{C}. Thus, for $a = 12$, higher stress values are required for plastic deformation to occur.

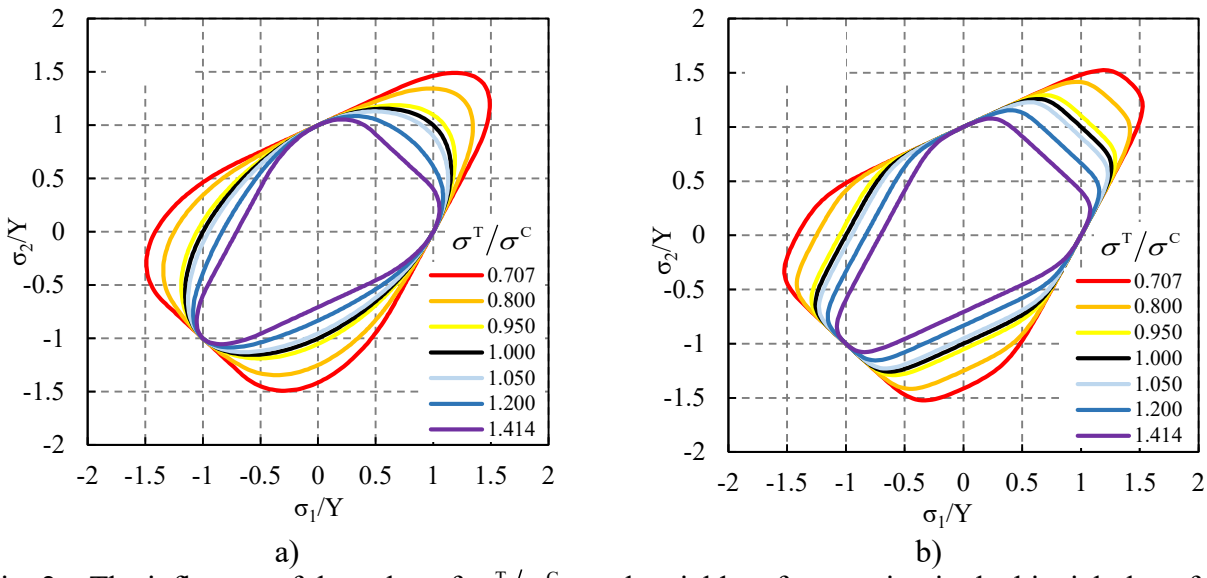

Fig. 2 – The influence of the value of σ^{T}/σ^{C} on the yield surface section in the biaxial plane for: a) $a = 2$ and b) $a = 12$. The principal stresses are normalized by the yield stress in uniaxial tension.

Table 1 – Selected values of σ^{T}/σ^{C} and corresponding k values.

σ^{T}/σ^{C}	k $(a=2)$	σ^{T}/τ $(a=2)$	k $(a=12)$	σ^{T}/τ $(a=12)$
0.707	-1	1.500	-0.17285	1.502
0.800	-0.375759	1.568	-0.1114	1.508
0.950	-0.07733	1.689	-0.02567	1.555
1.000	0	1.732	0	1.589
1.050	0.073523	1.775	0.024415	1.634
1.200	0.293848	1.913	0.091087	1.816
1.414	1	2.121	0.172856	2.124

The projection of the yield surface in the biaxial plane allows the evaluation of the normal vector, $\mathbf{n}$, at each point. When an associated flow rule is adopted, this normal defines the direction of the plastic strain rate tensor. In this particular case, the normal vector defines the ratio between the increment of plastic strain in the two principal directions ε_1 and ε_2. However, for some stress states $\varepsilon_1 > \varepsilon_2$ while for others $\varepsilon_1 < \varepsilon_2$. Thus, in order to be coherent, in the following analysis the in-plane minor strain $\varepsilon_{\text{minor}}$ is considered. The ratio between this strain and the one in the normal direction to

this plane, $\varepsilon_{\text{minor}}/\varepsilon_3$, is determined based on the volume conservation law. An auxiliary variable is defined which is the angle related with the considered stress state, i.e. loading direction φ (see Fig. 5 b)). This angle corresponds to the one associated to the slope between σ_1 axis and the considered stress state, such that for tension along the direction 1 its value is 0º, while for compression in the same direction it is 180º.

Fig. 3 a) presents the evolution of the strain ratio $\varepsilon_{\text{minor}}/\varepsilon_3$ in function of the loading direction, obtained analytically from the yield function, for the extreme $\sigma^{\text{T}}/\sigma^{\text{C}}$ values with $a=2$. Whatever the $\sigma^{\text{T}}/\sigma^{\text{C}}$ ratio considered, the strain ratio $\varepsilon_{\text{minor}}/\varepsilon_3$ is always equal to 1.0, for the loading directions of 0° (360°), 90°, 180°, 270°, which for the first two angles means uniaxial tension and for the two latter uniaxial compression. The strain ratio of 1.0 is the one expected for isotropic materials, submitted to either tension or compression. Moreover, whatever the $\sigma^{\text{T}}/\sigma^{\text{C}}$ ratio considered, for the loading directions of 45° and 225°, the value of the strain ratio is -0.5, because they correspond to biaxial tension and compression, for which $\varepsilon_1=\varepsilon_2$. However, due to the triangle-like shape with the "tip" in opposite directions, according to the $\sigma^{\text{T}}/\sigma^{\text{C}}$ ratio considered, this will lead to different trends for the plane strain states. These states correspond to $\varepsilon_{\text{minor}}/\varepsilon_3=0$. Fig. 3 a) shows that for $\sigma^{\text{T}}/\sigma^{\text{C}}>1$, this condition occurs for loading directions closer to uniaxial tension (0º and 90º) and biaxial compression (225º), when compared with the von Mises material. The opposite occurs for $\sigma^{\text{T}}/\sigma^{\text{C}}<1$, i.e. the condition $\varepsilon_{\text{minor}}/\varepsilon_3=0$ occurs for loading directions closer to biaxial tension (45º) and uniaxial compression (180º and 270º), when compared with the von Mises material.

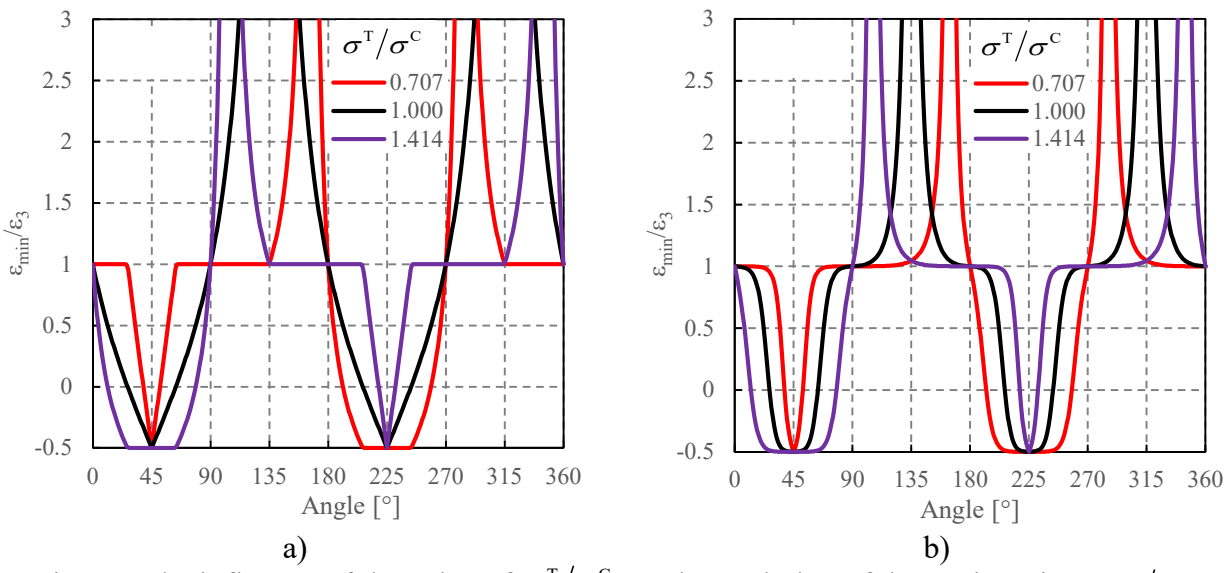

Fig. 3 – The influence of the value of $\sigma^{\text{T}}/\sigma^{\text{C}}$ on the evolution of the strain ratio $\varepsilon_{\text{minor}}/\varepsilon_3$: a) $a=2$ and b) $a=12$.

The shear stress states correspond to loading direction angles of 135º and 315º for the von Mises material, which correspond to an asymptote since $\varepsilon_3=0$. Fig. 3 a) shows that for $\sigma^{\text{T}}/\sigma^{\text{C}}>1$, the condition $\varepsilon_3=0$ occurs for loading directions closer to uniaxial tension, when compared with the von Mises yield criterion, while for $\sigma^{\text{T}}/\sigma^{\text{C}}<1$, it occurs for loading directions closer to uniaxial compression. Thus, the shear stress state $(\sigma_1=-\sigma_2)$ does not imposes the iso-thickness condition.

Fig. 3 b) presents the evolution of the strain ratio $\varepsilon_{\text{minor}}/\varepsilon_3$ in function of the loading direction, obtained analytically from the yield function, for the extreme $\sigma^{\text{T}}/\sigma^{\text{C}}$ values and a material with no SD effect for $a=12$. Globally, the trends are similar to the ones previously discussed, with more evident differences for $\sigma^{\text{T}}/\sigma^{\text{C}}=1$, since the evolutions are smoother than for $a=2$.

Numerical Simulation of the Cylindrical Cup Forming

The geometry of the tools selected for the cylindrical cup problem have the dimensions indicated in Fig. 4. The blank is circular with a diameter of 120 mm and a nominal thickness of 1.0 mm. In

order to minimize the occurrence of stress components normal to the sheet plane in the flange region, the simulations were performed considering a constant value for the gap between the blank-holder and the die. In order to avoid the occurrence of any ironing of the cup's wall, the punch height was assumed equal to 17 mm, i.e. the gap of 1.2 mm between the punch and the die is only valid on the prescribed height (see Fig. 4). The contact between sheet and tools is assumed frictionless.

The elastic behaviour is assumed isotropic, with a Young modulus E=210 GPa and a Poisson ratio ν=0.3. The hardening behaviour is considered to be isotropic, described by a power-law, such that $Y = 529.6(0.0044+\bar{\varepsilon}^{\mathrm{p}})^{0.268}$ MPa where $\bar{\varepsilon}^{\mathrm{p}}$ is the equivalent plastic strain. The adopted values result in an initial yield stress of 123.7 MPa. Nevertheless, it should be mentioned that the hardening law has a minor influence on the cup height and thickness distribution, which are mainly affected by the shape of the yield locus [2].

The tools were described with Nagata Patches [3]. The blank was discretized with 2D axisymmetric elements, due to geometrical and material symmetries. A total of 1280 quadrilateral elements was used, which correspond to four layers of elements through the thickness. The element type used is quadratic, with 9 nodes, combined with a full integration technique (4 Gauss points, per element). All numerical simulations are performed with the in-house code DD3IMP (Deep Drawing 3D IMPlicit) [3,4].

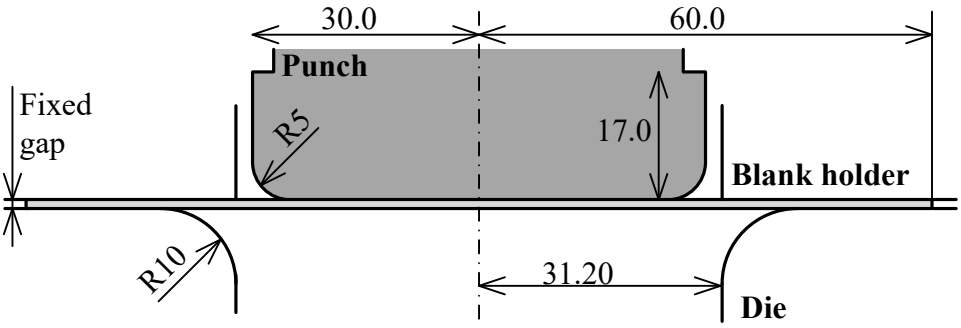

Fig. 4 – Schematic representation of the forming tools used in the cup drawing simulations (dimensions in mm) [2].

In terms of results analysis, it should be mentioned that for isotropic sheets, the rolling direction (RD) could be any reference direction in the sheet plane. In this case, this reference direction is assumed coincident with θ=0°, as shown in Fig. 5. The transverse direction (TD) is the direction normal to RD in the plane of the sheet, while the normal direction (ND) is normal to the plane of the sheet. In the analysis, two coordinate systems are utilized as presented in Fig. 5. One is the Cartesian orthogonal system, defined by RD; TD; ND, and the other is the cylindrical coordinate system, that is more appropriate for analysing the geometry of the cup, defined by the radial (r), the circumferential (θ) and the perpendicular direction (z). Note that since the material is isotropic, it is sufficient to analyse the mechanical response for materials points located along the RD direction.

The analysis of the results is focused on the evolution of the punch force with its displacement and of the thickness distribution. In addition, the evolution of the stress and strain states is analysed for the top and bottom surface of the cup. This analysis is performed for Gauss points (see Fig. 5 c)), with initial coordinates selected such that they are located in the centre of the cup (bottom), on the transition between the punch radius and the vertical wall and along the vertical wall. The selected points have initial coordinate R_0 = 0, 30, 42, 48, 54, 60 mm.

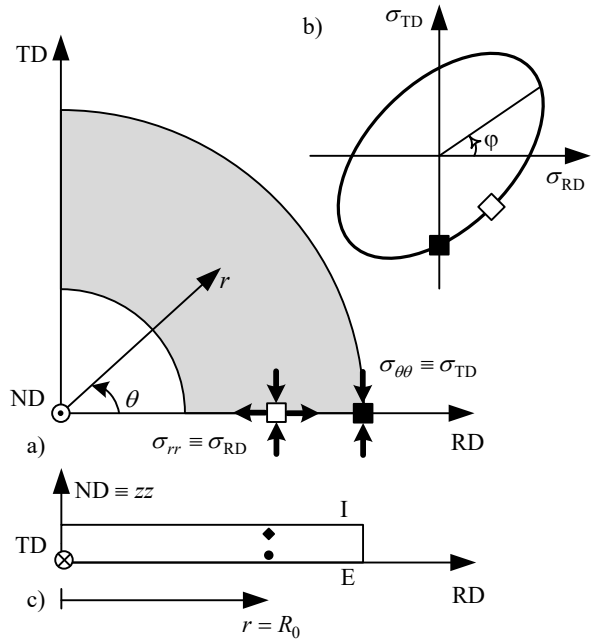

Fig. 5 – Analysis of the stress states for material points located in the flange: a) definition of the coordinate systems; b) schematic representation of the stress states on the cross-section of the yield surface (adopted from Yoon et al. [5]); and c) position of the material points considered for the analysis of the strain and stress paths (note that the blank thickness is exaggerated) [2].

Analysis of the Finite Element Results and Discussion

Drawing force. Fig. 6 presents the evolution of the punch force with its displacement for the selected stress ratios and $a = 2$ and $a = 12$. Note that the highest value of the force is predicted for the material with $\sigma^{T}/\sigma^{C} = 0.707$ and the lowest for $\sigma^{T}/\sigma^{C} = 1.414$. This is in accordance with the projection of the yield surface (see Fig. 2), which shows that the most exterior surface occurs for the lowest σ^{T}/σ^{C} ratio, what implies that more energy is required to promote the plastic deformation of that blank.

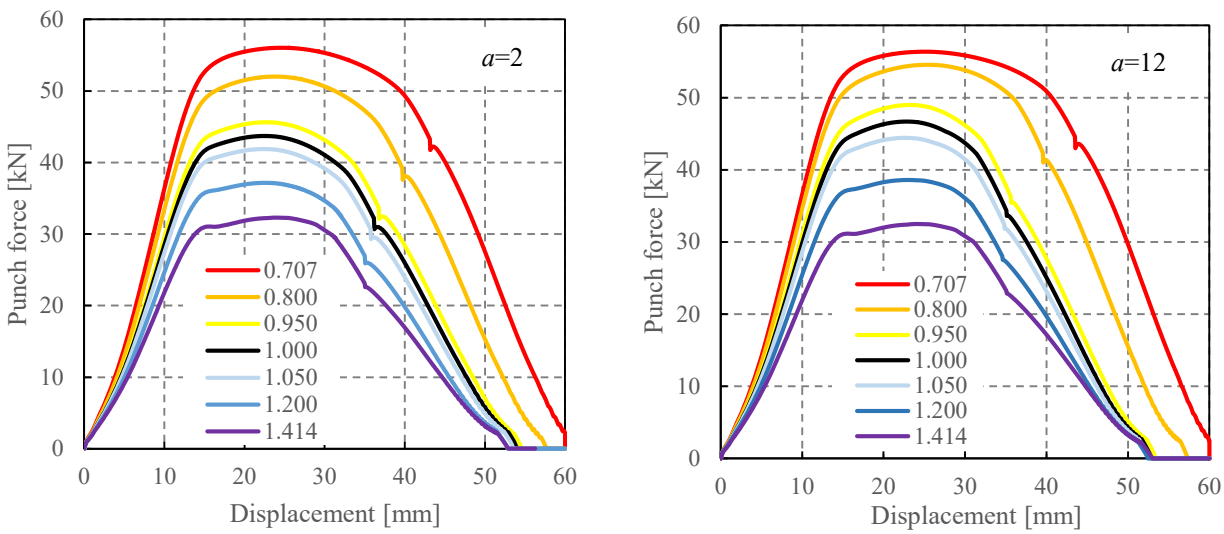

a) b)

Fig. 6 – The influence of the value of σ^{T}/σ^{C} on the punch force evolution for: a) $a = 2$ and b) $a = 12$.

The influence of the cup height is also visible in the punch force evolution. First, it affects the displacement for which the blank lost contact with the blank-holder (location of a slight, but sudden

drop in force). This occurs for a punch displacement between 35 and 45 mm, depending on σ^{T}/σ^{C}, being higher for lower values of this ratio. It should be noticed that the maximum force value for σ^{T}/σ^{C} =1 is higher for $a=12$. This is in accordance with the fact the yield surface for $a=12$ is exterior to the one obtained with $a=2$, as shown in Fig. 2. For materials with $\sigma^{T}/\sigma^{C}>1$, the results show a smaller influence of a, while for $\sigma^{T}/\sigma^{C}<1$ the maximum force tends to be higher for $a=12$.

Cup geometry. Fig. 7 presents the thickness distribution along the wall of the fully drawn cups (i.e. at the end of the forming process). All cups present a uniform thickness in the flat bottom (curvilinear distance between 0 and 25 mm), lower than the initial one (thinning). In the zone corresponding to the punch shoulder radius (curvilinear distance between 27 and 33 mm), the thickness presents a decrease. The vertical wall is characterized by thickness values higher than the initial one (thickening) for σ^{T}/σ^{C} values higher than 1 and slightly lower than 1. Notice that all material points located at an initial distance from the cup's centre higher than 30 mm have to reduce their radius, which means that they are submitted to compression in the circumferential direction (θ). However, the thickness variation in the cup wall is strongly dependent on σ^{T}/σ^{C}. The trend is similar for σ^{T}/σ^{C} values higher than 1 and values slightly lower than 1. For $\sigma^{T}/\sigma^{C}>0.8$, the lower thickness values occur in the zone corresponding to the transition between the flat bottom and the punch shoulder. These cups also present the lowest thickness values in the cup bottom and the highest in the vertical wall. For $\sigma^{T}/\sigma^{C}\leq 0.8$, the lower thickness values occur in the vertical wall. These cups also present the highest thickness in the cup bottom and the lowest in the vertical wall. In fact, the highest differences, particularly in the thickness along the cup wall, are observed for $\sigma^{T}/\sigma^{C}\leq 0.8$, which can correspond to more than 20% of thinning for lowest σ^{T}/σ^{C} ratio. On the other hand, for the highest σ^{T}/σ^{C} value, a significant difference is only observed at the cup's bottom. In fact, it should be mentioned that the difference between the two extreme values of σ^{T}/σ^{C} in the bottom is around 0.16 mm. However, the lowest σ^{T}/σ^{C} is the one presenting higher thinning, meaning that it would be more probable that the component would be rejected.

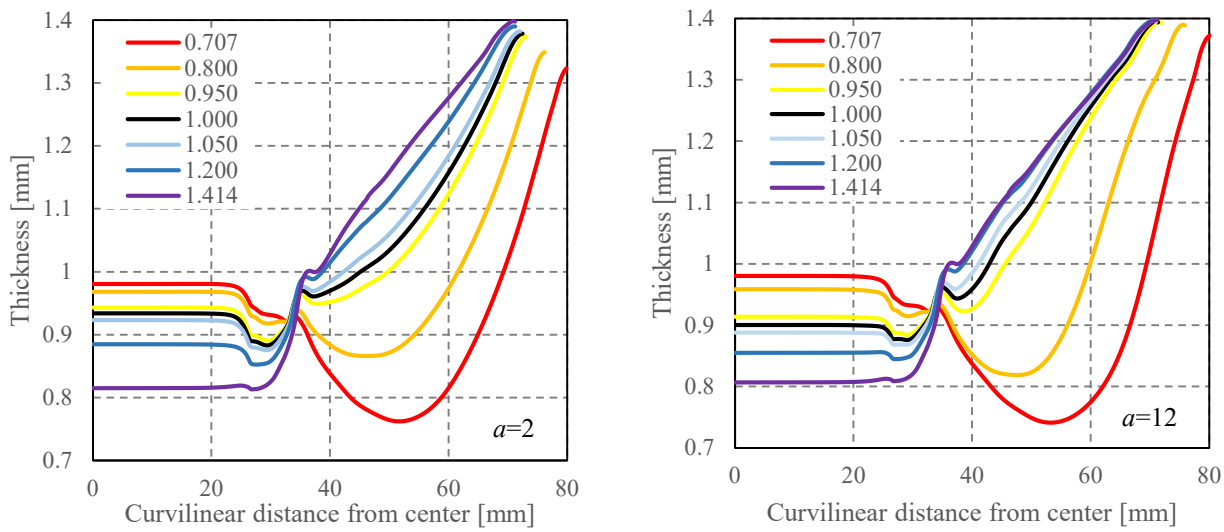

a) b)

Fig. 7 – The influence of the value of σ^{T}/σ^{C} on the thickness distribution for: a) $a=2$ and b) $a=12$.

Fig. 8 a) presents the cup height predicted at the end of the forming process as a function of the SD effect. As observed in Fig. 7, the highest cups are obtained with the lowest stress ratio. As the σ^{T}/σ^{C} ratio increases, the height quickly drops becoming almost constant for material with a ratio around 1.1 and higher. Moreover, the difference in the predicted cup height, for σ^{T}/σ^{C} from ~0.7 to ~1.4, is around 8 mm (~20%). Fig. 8 b) presents the profiles of the formed cups for the two extreme σ^{T}/σ^{C} ratios and for the isotropic von Mises material, to help understanding the relation between

the thickness distribution and the cup height. Notice that the cup with σ^{T}/σ^{C} =1.414 has the most uniform increase of thickness along the vertical wall. The results of Fig. 8 are consistent with the displacement for which the punch force is null (Fig. 6). The difference in the predicted cup height for $a=2$ and $a=12$ is more relevant for σ^{T}/σ^{C} closer to 1, while for the extreme values of σ^{T}/σ^{C} ratios it is negligible. This is in agreement with the analysis of the influence of the parameter a in the shape of the yield surface (Fig.2). Globally, for the same σ^{T}/σ^{C} ratio, the cup is higher for $a=2$.

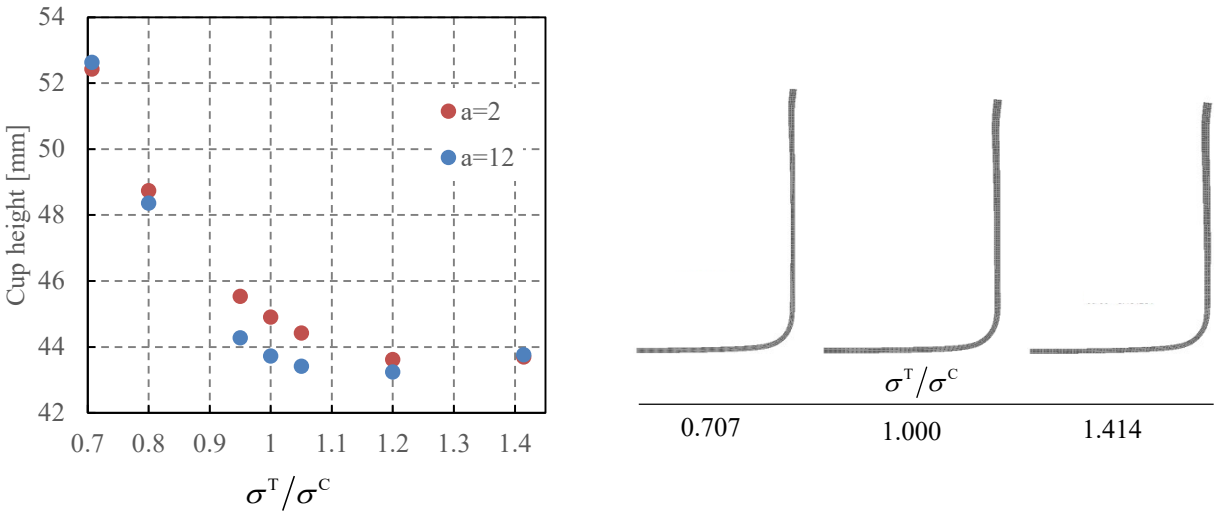

a) b)

Fig. 8 – The influence of the value of σ^{T}/σ^{C} on the cup height:
a) trend for $a=2$ and $a=12$; b) predicted geometry for $a=2$.

Points for strain and stress analysis. As shown schematically in Fig. 5, the points located on the exterior side of the flange (initial radius R_0 = 60 mm) are subjected to compression in the θ direction, while the interior points (i.e. with smaller R_0 values) are subjected to tension in the radial direction, and compression in the circumferential direction; the ratio between the circumferential $(\sigma_{\theta\theta} \equiv \sigma_{\mathrm{TD}})$ and the radial $(\sigma_{rr} \equiv \sigma_{\mathrm{RD}})$ stress components depends on the location along the RD.

The process conditions adopted are such that the punch is initially located at z = 1 mm, and it moves downward (negative z values). The analysis of the stress and strain paths is performed for Gauss points located on top and bottom surfaces of the flange (see Fig. 5 c)). The material points initially located on the top surface of the flange that end up in the interior part of the cup are referred to as the top, the material points which are initially located on the bottom surface of the flange that end up on the exterior part are referred to as bottom.

The Gauss points selected to analyse the behaviour of the flange material are initially located between R_0 = 60 mm (outer surface) and R_0 = 42 mm, with increments of 6 mm. The other points selected present an initial radius of R_0 = 0 mm and R_0 = 30 mm, to help understanding the behaviour of the material located in the cup' bottom and in the transition between the punch shoulder radius and the vertical wall. In the beginning of the process, the points located at R_0 = 30 mm are submitted to bending, but after a punch displacement of approximately 20 mm its position remains almost unaltered. The points at R_0 = 42, 48, 54, 60 mm change their position from the flange to the vertical wall. For instance, the points at R_0 = 42 mm are in the zone of influence of the die shoulder for a punch displacement of 5 mm and end-up with a curvilinear distance from the centre of the cup between 48 and 42 mm (see Fig. 7). The detailed analysis of the stress and strain states is performed only for the lowest and highest stress ratio σ^{T}/σ^{C} and for the one that corresponds to von Mises criterion, i.e. $a=2$.

Strain paths. Fig. 9 shows the strain paths of the selected points during the forming process. To better understand the differences, the analysis is performed first for the von Mises material (σ^{T}/σ^{C} =1). For this material, the uniaxial compression stress state is defined by $\varepsilon_{\mathrm{minor}} = -2\varepsilon_{\mathrm{major}}$.

This is the ratio observed for the material points located at R_0 = 60 mm, which corresponds to the ones closest to the outer surface of the blank, which are submitted only to compression in the circumferential direction. The shear stress state is defined by $\varepsilon_{\text{minor}} = -\varepsilon_{\text{major}}$.

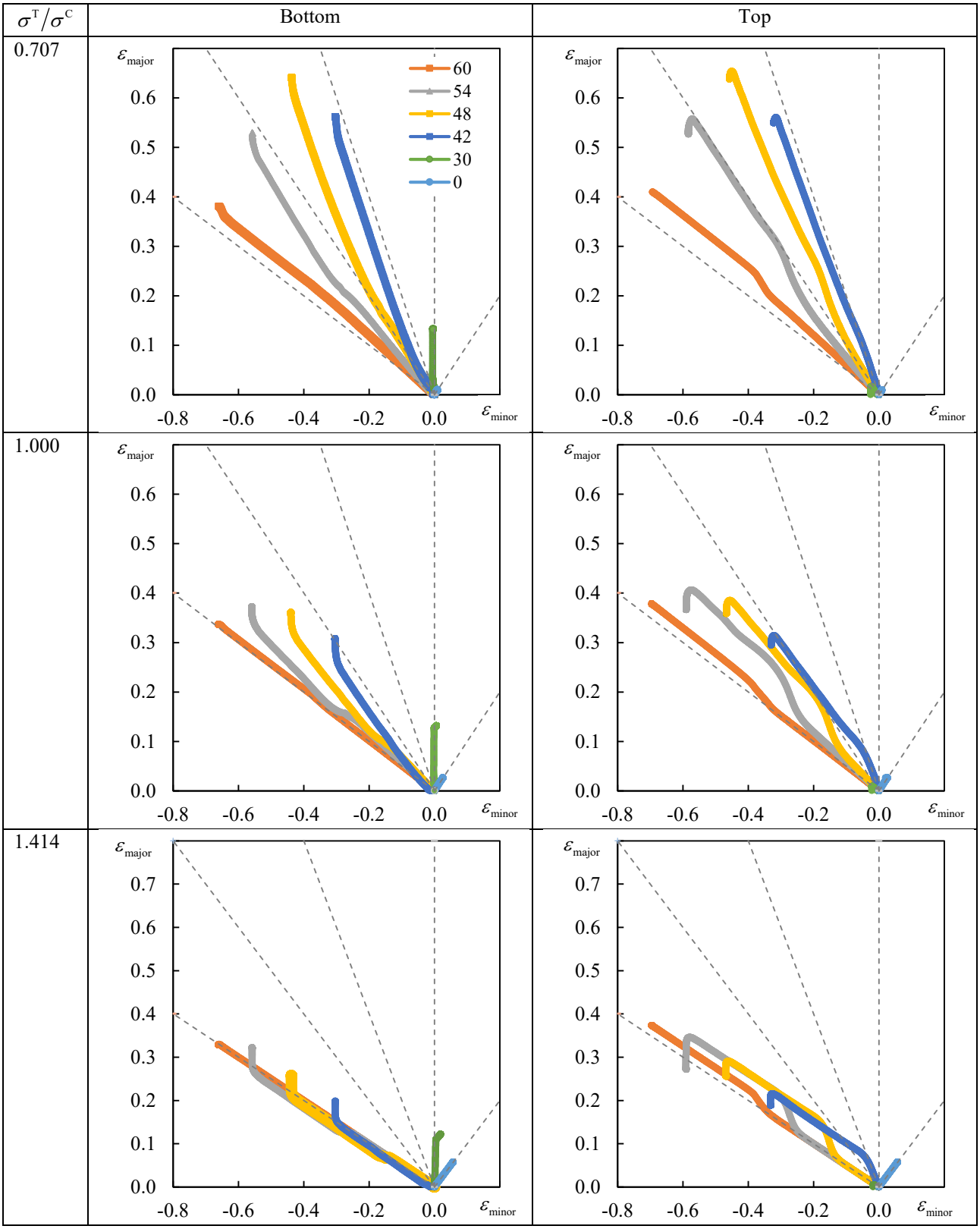

Fig. 9 – Strain paths (for integration points located close to top and bottom cup surface) obtained for materials characterized by different tension-compression ratios in comparison with a von Mises material, for $a = 2$.

All the other points initially located in the flange present a strain path, between uniaxial compression and shear stress states (see dashed lines). For the points located in the top, the subtle change between the compression and the shear stress states is more evident, which can be associated with the tension stress imposed by the bending over the die shoulder radius. The uniaxial tension is defined by $\varepsilon_{\text{minor}} = -\varepsilon_{\text{major}}/2$, which is never attained. At the end of the forming process, the strain path of the points originally located in the flange change to plane strain state ($\varepsilon_{\text{minor}} = 0$), since their diameter is already defined and they are mainly being submitted to uniaxial tension, imposed by the punch movement. The points located at R_0 = 30 mm present also a plane strain path, although it is clearly more visible for the one in the bottom, since it attains higher values of equivalent plastic strain, imposed by the bending in the punch shoulder radius. This also seems to promote the change to a strain path close to equibiaxial tension. Finally, the equibiaxial tension condition is defined by $\varepsilon_{\text{minor}} = \varepsilon_{\text{major}}$, this corresponds to the strain path observed for the points located at R_0 = 0 mm.

Note that for isotropic materials, the principal directions for stresses and strains coincide. Thus, it can be considered that for the material points analysed on the three cups: $\varepsilon_{\theta\theta} \equiv \varepsilon_{\text{TD}}$ and $\varepsilon_{rr} \equiv \varepsilon_{\text{RD}}$. Globally, when comparing the different materials, they present similar values for $\varepsilon_{\text{minor}}$. This is consistent with the fact that this corresponds to the strain in the circumferential direction, which is mainly dictated by the tools geometry. The maximum value it close to $\ln(30/60) = -0.69$. On the other hand, the material with the lower $\sigma^{\text{T}}/\sigma^{\text{C}}$ ratio attains the highest values for the $\varepsilon_{\text{major}}$, for the points originally located in the flange. The opposite occurs for the material with the higher $\sigma^{\text{T}}/\sigma^{\text{C}}$ ratio. Moreover, the points originally located in the flange demonstrate different slopes for the strain paths for the material with the lower $\sigma^{\text{T}}/\sigma^{\text{C}}$. On the other hand, for the material with the higher $\sigma^{\text{T}}/\sigma^{\text{C}}$, the slope is almost equal for all points. Remind also that the condition $\varepsilon_{\text{minor}} = -\varepsilon_{\text{major}}$ corresponds to the iso-thickness condition, i.e. $\varepsilon_3 = \varepsilon_{\text{ND}} = 0$. The strain states below this line correspond to thickening and the ones above to thinning. Only the material with the lower $\sigma^{\text{T}}/\sigma^{\text{C}}$ ratio attains strain paths corresponding to the thinning region, which is consistent with the lower thickness values reported in Fig. 7. For the points at R_0 = 30 mm, the strain paths are quite similar, for all materials, although the change for the equibiaxial strain path is more evident for the material with the higher $\sigma^{\text{T}}/\sigma^{\text{C}}$. For the points at R_0 = 0 mm, the strain paths are quite similar, for all materials, but the strain values attained increase with the increase of the $\sigma^{\text{T}}/\sigma^{\text{C}}$ ratio. These results are consistent with the higher thinning observed in Fig. 7.

Stress paths. The stress states were also analysed for the same integration points. However, their comparison with the reference yield surfaces, presented in Fig. 2, poses additional challenges, because they can only be presented while all other components of the Cauchy stress tensor are negligible when compared to the ones considered ($\sigma_1 = \sigma_{rr}$; $\sigma_2 = \sigma_{\theta\theta}$). Moreover, they are only plotted when an increment in the equivalent plastic strain is observed, to avoid the representation of states that correspond to an unloading to the elastic regime. Thus, in the following analysis, one needs to consider that the stress states were only plotted for increments that fulfil this condition. The stress tensor that was analysed corresponds to the one defined in the material axis, according with the definition presented in Fig. 5. The components analysed are the ones corresponding to RD and TD directions ($\sigma_1 = \sigma_{\text{RD}}$; $\sigma_2 = \sigma_{\text{TD}}$), which were normalized with the flow stress value, in order to take into account the hardening behaviour.

Fig. 10 presents the stress states extracted for the Gauss points under analysis. The material points located at R_0 = 0 mm present an equibiaxial stress state. Note that for the lower $\sigma^{\text{T}}/\sigma^{\text{C}}$ ratio, the point on the top starts to deform under equibiaxial compression then, moves to an elastic state (not presented in the figure) and, only afterwards, deforms under equibiaxial tension. The first change to a plastic state occurs when the point of the bottom also deforms, but while the later continues to deform, the point on the top stops and only continues to deform for a punch displacement of approximately 5 mm. This is certainly a result of the high value of equibiaxial stress, as shown in Fig. 2. The material point located at R_0 = 30 mm in the bottom is mainly in a plane strain state, while the one located in the top is mainly in uniaxial compression. Nevertheless, this allows us to assume that the points located in the bottom of the cup, in the bottom surface, present stress states between equibiaxial tension and plane strain.

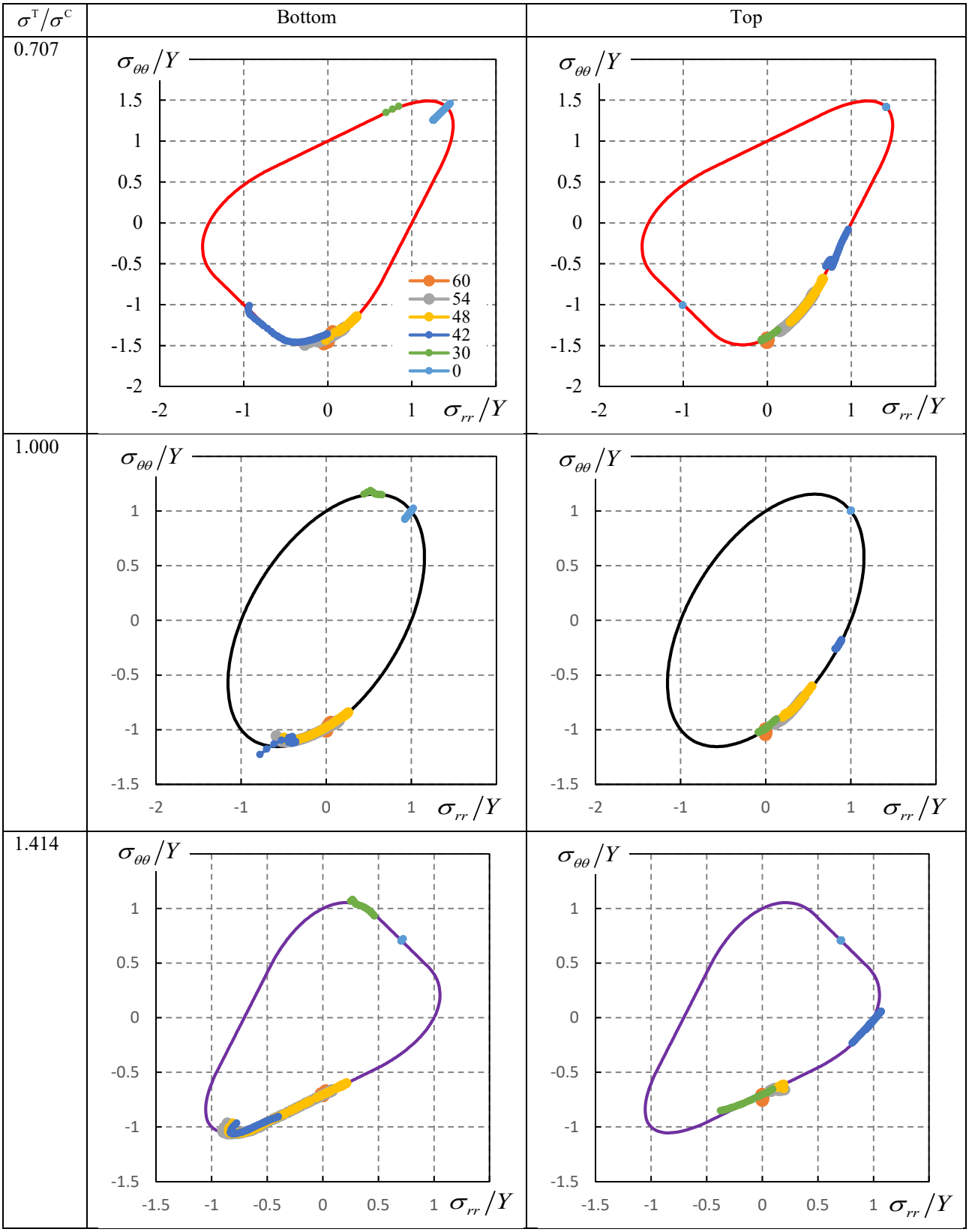

Fig. 10 – Stress paths (for integration points located close to top and bottom cup surface) obtained for materials characterized by different tension/compression ratios in comparison with a von Mises material, for $a = 2$.

Fig. 3 shows that the evolution of the strain ratio $\varepsilon_{\min}/\varepsilon_3$ is quite different, for the three materials, for these loading directions. In particular, the material with the lowest σ^T/σ^C ratio shows a sharp variation of the $\varepsilon_{\min}/\varepsilon_3$ ratio, while the material with the highest σ^T/σ^C ratio presents an almost constant value of - 0.5. Thus, for similar values of ε_{rr} ($= \varepsilon_{\text{major}}$ in Fig. 9), the points located in the cup

bottom will deform more in the thickness direction, for the material with the highest σ^{T}/σ^{C} ratio. Moreover, since the in-plane strain is positive, the $\varepsilon_{min}/\varepsilon_3$ ratio of -0.5 imposes thinning, which helps justifying the lowest thickness values in the cup bottom for the material with the highest σ^{T}/σ^{C} ratio (see Fig. 7). On the other hand, the sharp variation of the $\varepsilon_{min}/\varepsilon_3$ ratio leads to lower thickness strains, justifying the highest thickness values in the cup bottom for the material with the lowest σ^{T}/σ^{C} ratio.

Regarding the material points located initially in the flange, they present a stress state that starts close to the uniaxial compression, particularly the point located in the outer surface. The others present a positive component for the stress component in the radial direction (see Fig. 5). That is why the stress path becomes closer to the shear stress state. When the material points approach the zone of influence of the die shoulder radius, the bending induces compressive stress for the bottom points and tensile ones for the points on the top. That is why for the bottom points one can observe the change from the forth to the third quadrant, including the occurrence of a plane strain state. On the other hand, for the points in the top, the tendency to remain in the fourth quadrant is more evident.

Note that for the material with the lowest σ^{T}/σ^{C} ratio, the material point located in the bottom surface at $R_0 = 42$ mm presents an equibiaxial compression stress state. It is also important to mention that, all materials present a ratio between the in-plane strains equal to -2 for uniaxial compression, since they are all isotropic. The material with the highest σ^{T}/σ^{C} ratio, presents a value of -2 for a wide range of loading directions, since the compression plane strain changes its location (Fig. 3). This explains why the strain paths remain almost constant for all points located in the flange and why the strains in the radial direction are smaller (see Fig. 9). On the other hand, the material with the lowest σ^{T}/σ^{C} ratio, presents a sharp change for the ratio between the in-plane strains, attaining a value of -0.5 for the loading direction of 315°, since both the compression plane strain and the shear strain states change their location (Fig. 3). This explains why the strain paths change so much for the points located in the flange and also why the strains in the radial direction are larger (see Fig. 9). Moreover, this also explains why a material points initially located between $R_0 = 48$ mm and $R_0 = 54$ mm can present no thickness change for the material with the lowest σ^{T}/σ^{C} ratio, while for the other materials there is a thickening (see also Fig. 7).

In resume, the points on the bottom side present loading directions somewhere between angles of 225° and 315°. The points of the top are roughly between 270° and 360°, except for higher stress ratios where the range starts from angles smaller than 270°. The $\varepsilon_{min}/\varepsilon_3$ ratio is positive for all stress ratio between plane strain in compression ($|\sigma_{\theta\theta}| > |\sigma_{rr}|$) and plane strain in tension ($|\sigma_{rr}| > |\sigma_{\theta\theta}|$). It is necessary to be more careful in this analysis, due the proper identification of ε_{min}. Thus, focus is given only to the stress states that present higher compression in the circumferential direction than tension in the radial direction. This means that ε_{min} is positive and, according to Fig. 3, also $\varepsilon_3 > 0$, meaning that an increase of thickness occurs. Fig. 3 shows that for loading directions around the uniaxial compression, the material with the higher σ^{T}/σ^{C} ratio presents a constant value for the $\varepsilon_{min}/\varepsilon_3$ ratio. This explains why the points located in the flange have all very similar strain paths (see Fig. 9), although the loading direction is different. On the other hand, the material with the smaller σ^{T}/σ^{C} ratio presents a sharp variation of the $\varepsilon_{min}/\varepsilon_3$ ratio. This confirms the different strain paths shown in Fig. 9. The material points present similar values for the circumferential strain ($= \varepsilon_{\theta\theta}$ in Fig. 9). For the material with the higher σ^{T}/σ^{C}, the constant ratio results in a lower strain in the radial direction, when compared to the one observed for the smallest σ^{T}/σ^{C} ratio. This also helps justifying the more uniform distribution of the thickness along the cup wall, for the material with the higher σ^{T}/σ^{C} ratio (see Fig. 7). The opposite occurs for the material with the smallest σ^{T}/σ^{C} ratio, leading to higher cups. In resume, although all materials are isotropic, the SD effect will lead to different cup geometries, due to the different distributions of the thickness, when assuming an associated flow rule.

Although the analysis of the strain and stress paths is only performed for $a = 2$, it also helps understanding the differences observed for $a = 12$. Fig. 7 shows that for all materials the differences in the bottom part of the cup are negligible. However, in the cup wall the trend obtained is more similar for the materials with $a = 12$ and $\sigma^{T}/\sigma^{C} \geq 1$. This is in agreement with the analysis of the

strain ratios presented in Fig. 3. For $a = 12$ there is a smoother variation of the $\varepsilon_{\min}/\varepsilon_3$ ratio. Thus, the trend observed for $a = 2$ is maintained but with a more uniform distribution, for $\sigma^{\mathrm{T}}/\sigma^{\mathrm{C}} \geq 1$. On the other hand, for the materials with $\sigma^{\mathrm{T}}/\sigma^{\mathrm{C}} < 1$ and $a = 12$ the plateaus with constant $\varepsilon_{\min}/\varepsilon_3$ ratio are narrower, leading to a more uneven distribution of the thickness along the cup wall.

Conclusions

The Cazacu et al. (2006) yield function is not an even function in stresses, which means that it can capture the tension–compression asymmetry demonstrated by some materials. In this work, the aforementioned yield criterion was applied to study the influence of the tension–compression asymmetry on the forming of a cylindrical cup, for materials presenting isotropic behaviour. Numerical simulations of the deep drawing of a cylindrical cup were conducted considering isotropic materials with different $\sigma^{\mathrm{T}}/\sigma^{\mathrm{C}}$ ratios. The results show that even small changes in the $\sigma^{\mathrm{T}}/\sigma^{\mathrm{C}}$ ratio have impact in the punch force and in the cup final geometry. Cups with a higher height are obtained for $\sigma^{\mathrm{T}}/\sigma^{\mathrm{C}}$ ratios lower than 1. This results from the fact that these cups present a less uniform distribution of the thickness along the cup wall. In fact, for low values of $\sigma^{\mathrm{T}}/\sigma^{\mathrm{C}}$ the wall can present thickness values lower than the one attained with the von Mises material, becoming the critical point of the component. The thickness distributions obtained are a consequence of the shape of the yield surface, particularly for stress states located close to uniaxial compression. The materials considered in this work are all virtual, since the aim was to understand the impact of the SD effect. The results show that even small changes in the $\sigma^{\mathrm{T}}/\sigma^{\mathrm{C}}$ ratio can influence the strains distribution, in isotropic materials. This can be particularly relevant for loading conditions involving compression states, but also shear, plane strain and equibiaxial tension or compression. In this context, it is important to improve the knowledge about the $\sigma^{\mathrm{T}}/\sigma^{\mathrm{C}}$ ratio for materials, which are commonly accepted to present an isotropic behaviour.

Acknowledgements

The authors gratefully acknowledge the financial support of the projects POCI-01-0145-FEDER-30592 (PTDC/EME-EME/30592/2017) and UIDB/00285/2020 financed by the Operational Program for Competitiveness and Internationalization, in its FEDER/FNR component, and the Portuguese Foundation of Science and Technology (FCT), in its State Budget component (OE).

References

[1] O. Cazacu, B. Plunkett, F. Barlat, Orthotropic yield criterion for hexagonal closed packed metals, Int. J. Plast. 22 (2006) 1171–1194. https://doi.org/10.1016/j.ijplas.2005.06.001.

[2] M.C. Oliveira, O. Cazacu, N. Chandola, J.L. Alves, L.F. Menezes, On the effect of the ratio between the yield stresses in shear and in uniaxial tension on forming of isotropic materials, Mech. Res. Commun. 114 (2021) 103693. https://doi.org/10.1016/J.MECHRESCOM.2021.103693.

[3] D.M. Neto, M.C. Oliveira, L.F. Menezes, Surface Smoothing Procedures in Computational Contact Mechanics, Arch. Comput. Methods Eng. 24 (2015) 37–87. https://doi.org/10.1007/s11831-015-9159-7.

[4] L.F. Menezes, C. Teodosiu, Three-dimensional numerical simulation of the deep-drawing process using solid finite elements, J. Mater. Process. Technol. 97 (2000) 100–106. https://doi.org/10.1016/S0924-0136(99)00345-3.

[5] J.W. Yoon, R.E. Dick, F. Barlat, A new analytical theory for earing generated from anisotropic plasticity, Int. J. Plast. 27 (2011) 1165–1184. https://doi.org/10.1016/j.ijplas.2011.01.002.